Bioresource Technology 245 (2017) 1634–1640

Contents lists available at ScienceDirect

Bioresource Technology

journal homepage: www.elsevier.com/locate/biortech

Metabolic impact of nutrient starvation in mevalonate-producing *Escherichia coli*

Ami Masuda, Yoshihiro Toya, Hiroshi Shimizu *

Department of Bioinformatic Engineering, Graduate School of Information Science and Technology, Osaka University, 1-5 Yamadaoka, Suita, Osaka 565-0871, Japan

HIGHLIGHTS

- Sulfur starvation achieved highest mevalonate yield of 0.61 C-mol/C-mol in *E. coli*.
- Degradation of MvaE enzyme caused a large TCA cycle flux under nitrogen starvation.
- TCA cycle flux was suppressed under magnesium or sulfur starvation.
- Mevalonate synthesis was reduced by NADPH supply shortage under magnesium starvation.
- Low TCA cycle flux and enough NADPH production led high yield in sulfur starvation.

ARTICLE INFO

Article history:
Received 31 March 2017
Received in revised form 26 April 2017
Accepted 28 April 2017
Available online 4 May 2017

Keywords:
Mevalonate
Escherichia coli
Nutrient starvation
^{13}C-metabolic flux analysis

ABSTRACT

The aim of this work was to enhance mevalonate yield from glucose in *Escherichia coli* by essential nutrient starvations and to reveal these effects on the central carbon metabolism. Stationary phase culture without essential nutrients such as nitrogen, sulfur, and magnesium was evaluated using an engineered *E. coli* introducing *mvaE* and *mvaS* genes from *Enterococcus faecalis*. Sulfur starvation resulted in the highest mevalonate yield of 0.61 C-mol C-mol^{-1} from glucose. The metabolic impacts of nutrient starvation were investigated by ^{13}C-metabolic flux analysis. Under nitrogen starvation, the flux of the TCA cycle was large, causing high CO_2 production. This was caused by degradation of mevalonate synthesis pathway enzymes. Under magnesium starvation, NADPH production was decreased, which limited mevalonate synthesis and promoted an overflow of acetate. Sulfur starvation not only suppressed the TCA cycle flux, but also supplied NADPH for mevalonate synthesis.

1. Introduction

Mevalonate is a valuable precursor of terpenoids for drugs, cosmetics, fragrance, and coloring agents, and is an intermediate of a biosynthesis pathway for isoprenoids (Kuzuyama et al., 2004; Tabata and Hashimoto, 2004). This metabolite is synthesized from acetyl-CoA, the intermediate that links glycolysis to the TCA cycle, using NADPH as a cofactor. Mevalonate production has been studied in *Saccharomycopsis fibuligera*, which possesses a native mevalonate synthesis pathway, obtained by screening techniques (Tamura et al., 1968). *S. fibuligera* ADK8107, developed by Asahi Denka Co., Ltd. produced 19 g L^{-1} of mevalonate in 12 days (Kuzuyama et al., 2010). To further improve the productivity by metabolic engineering procedures, *Escherichia coli* has been used as a host because genetic manipulation is simple in this species (Tabata and Hashimoto, 2004). Because *E. coli* does not contain the mevalonate synthesis pathway, mevalonate synthesis genes derived from various species were introduced and mevalonate production was examined (Xiong et al., 2014). Heterologous expression of the mevalonate synthesis genes, *mvaE* and *mvaS*, derived from *Enterococcus faecalis* were used to achieve 47 g L^{-1} mevalonate production in 2 days (Tabata and Hashimoto, 2004). It has been reported that an *E. coli* strain expressing codon-optimized *mvaE* and *mvaS* under the T7 promoter produced mevalonate with a yield of 0.22 C-mol Cmol^{-1} during the exponential growth phase (Wada et al., 2017). Mass balance analysis suggested that there is no room for further mevalonate production at the biomass yield (Wada et al., 2017). Previous studies have suggested that mevalonate production can be enhanced by growth inhibition under sulfur starvation conditions (Li et al., 2016).

In bio-production, nutrient restriction can inhibit cell growth and lead to a stationary phase. Many nutrients are essential for *E. coli* growth, such as nitrogen, sulfur, phosphorus, and trace metal elements. It has been reported that metabolic state varies depends on the restricted nutrients in the parent strain (Chubukov and

* Corresponding author.
E-mail address: shimizu@ist.osaka-u.ac.jp (H. Shimizu).

http://dx.doi.org/10.1016/j.biortech.2017.04.110
0960-8524/

Sauer, 2014). For example, intracellular alpha-ketoglutarate (αKG) accumulates under nitrogen starvation conditions (Chubukov and Sauer, 2014). Because the phosphotransferase system is inhibited by αKG, glucose consumption rate is decreased (Doucette et al., 2011). Sulfur starvation suppresses the synthesis of amino acids containing thiol groups, and promotes decomposition of these amino acids (Shimizu, 2013). Furthermore, iron-sulfur (Fe-S) clusters are not produced under sulfur starvation conditions (Johnson et al., 2005). Because Fe-S clusters are required for various metabolic enzymes, the corresponding reactions are suppressed. Similarly, because magnesium is a cofactor of many metabolic enzymes, magnesium starvation would suppress various metabolic reactions (Chubukov and Sauer, 2014). However, the effects of such nutrient starvations on the metabolism of a mevalonate-producing strain remain unclear.

In the present study, mevalonate production was evaluated in a synthetic medium containing glucose as the sole carbon source without essential nutrients such as nitrogen, sulfur or magnesium using a mevalonate producing *E. coli* strain containing *mvaE* and *mvaS* from *E. faecalis*. The cause of the differences in mevalonate yield following restricted nutrition culture was investigated by ^{13}C-metabolic flux analysis (^{13}C-MFA).

2. Methods

2.1. Strains and medium

Escherichia coli K-12 MG1655(DE3) was used as the host strain. Codon-optimized *mvaE* and *mvaS* from *E. faecalis* were inserted into the multi-cloning site of the pCOLADuet-1 vector (Novagen). *E. coli* cells were transformed with this plasmid for mevalonate production by electroporation (Wada et al., 2017). *pntAB*, *sthA* and *zwf* were deleted by P1 phage transduction (Datsenko and Wanner, 2000). Gene deletions were confirmed by colony PCR using primers targeting sites upstream and downstream of the deletion (Table S1).

M9 medium (44.4 mM glucose, 47.2 mM Na_2HPO_4, 22.7 mM KH_2PO_4, 8.5 mM NaCl, 18.7 mM NH_4Cl, 1 mM $MgSO_4$, 0.05 mM $FeCl_3$, and 0.1 mM $CaCl_2$) supplemented with 1/1000 vol of trace metal solution (1 mg/L $MnCl_2$ $4H_2O$, 1.7 mg/L $ZnCl_2$, 0.43 mg/L $CuCo_2$ $2H_2O$, 0.60 mg/L $CoCl_2$ $6H_2O$, and 0.60 mg/L Na_2MoO_4 $2H_2O$) was used for cultivation. For nitrogen starvation, 18.7 mM NH_4Cl was removed. For magnesium starvation, 1 mM $MgSO_4$ was replaced with 1 mM Na_2SO_4. For sulfur starvation, 1 mM $MgSO_4$ was replaced with 1 mM $MgCl_2$ (Chubukov and Sauer, 2014).

2.2. Culture conditions

Cell concentration was measured as the absorbance at 600 nm (OD_{600}) using the UVmini-1240 (Shimadzu, Kyoto, Japan). Dry cell weight (DCW) was calculated using a conversion coefficient of 0.3 gDCW L^{-1} OD_{600}^{-1}. In preculture, a single colony was inoculated into 5 mL L medium in a test tube containing 30 mg/L kanamycin and cultured at 37 °C at 150 rpm for 17 h. The preculture was inoculated into 75 mL M9 medium in a 200-mL baffled flask at an OD_{600} of 0.05 and cultured at 37 °C at 150 rpm. At an OD_{600} of 0.5, isopropyl-β-d-thiogalactopyranoside was added to a final concentration of 0.1 mM. After 24 h, the cells were collected by centrifugation at 4000*g* for 5 min at room temperature and washed with M9 medium without glucose. The obtained cells were inoculated in 50 mL each nutrient-free medium in 200-mL baffled flask at OD_{600} of 9, and cultured at 37 °C at 150 rpm.

2.3. Measurement of extracellular metabolites

Concentrations of extracellular metabolites such as glucose, mevalonate, D-lactate, formate, acetate, succinate, and ethanol were measured by HPLC (Shimadzu) using an Aminex HPX-87H column (Bio-Rad, Hercules, CA, USA). Measurement conditions have been described previously (Wada et al., 2017).

2.4. SDS-polyacrylamide gel electrophoresis (SDS-PAGE)

An appropriate amount of cells ([OD_{600}] x culture volume [mL] = 30) was harvested by centrifugation at 15,000*g* for 10 min at 4 °C and the cell pellet was resuspended in 1 M Tris-HCl (pH 7.0). The cells were disrupted by sonication using a UD-100 sonicator (Tomy Seiko, Osaka, Japan) at an output of 50 with 5 s on/off cycles on ice. The samples were centrifuged at 20,000*g* for 5 min to remove debris. The total protein amount was quantified by Bradford assay (Bio-Rad). After denaturation at 95 °C for 3 min, the samples (containing 0.8 mg protein) were analyzed on a 10% SDS-PAGE gel. The gel was stained with Coomassie brilliant blue.

2.5. Measurement of intracellular cofactor levels

Cofactor levels were measured using EnzyChrom $NADP^+$/NADPH and NAD^+/NADH assay kits (BioAssay Systems, Hayward, CA, USA) according to the manufacturer's instruction. An appropriate amount of cells ([OD_{600}] × culture volume [mL] = 8) was harvested by centrifugation and the cell pellet was resuspended in 1 mL cold phosphate-buffered saline.

2.6. ^{13}C-labeling experiment

For flux estimation, the carbon source of the stationary phase medium was replaced with [1-^{13}C] glucose. The 3 mL culture was obtained at 2.5 and 3.5 h during the stationary phase, and was immediately quenched by mixing with 4 volumes of cold 60% (v/v) methanol containing 10 mM ammonium acetate. The quenched cells were collected by filtration using a PTFE membrane filter with 0.5 μm pore size (ADVANTECH, Taipei, Taiwan). After adding 640 μL of water and 1.6 mL of chloroform, the sample was mixed for 1 min and ultra-sonicated for 1 min, and then centrifuged 3700*g* for 20 min at 4 °C. The supernatant was evaporated at room temperature, and derivatized with *tert*-butyl dimethylsilylation (TBDMS) for pyruvate, αKG, phosphoenolpyruvate (PEP), citrate (Cit), and 3-phosphoglycerate (3PG) or trimethylsilylation (TMS) for fumarate (Fum), fructose 1,6-bisphosphate (FBP), and mevalonate.

For TBDMS derivatization, 50 μL of methoxyamine hydrochloride in pyridine (40 mg mL^{-1}) was added to the dried sample and incubated for 90 min at 37 °C. Then, 50 μL of *N*-Methyl-*N*-*tert*-butyldimethylsilyltrifluoroacetamide + 1% *tert*-butyldimethylchlorosilane was added and incubated for 30 min at 60 °C. Pyruvate (m/z = 174), αKG (m/z = 346), PEP (m/z = 453), Cit (m/z = 591), 3PG (m/z = 585), and their mass isotopomers were measured by gas chromatography mass spectrometry (GC/MS) (Agilent 7890A GC and 5975C MSD, Agilent Technologies, Santa Clara, CA, USA) in the selected ion monitoring mode under following conditions: column, DB-5MS + DG (30 m, 0.25 mm, 0.25 μm, Agilent Technologies); carrier gas, helium; inlet temperature, 250 °C; injection mode, split (1:10). Oven temperature was set as follows: 150 °C for 2 min, increased by 3 °C/min to 270 °C, and then increased by 10 °C/min to 300 °C maintained at 300 °C for 5 min. For TMS derivatization, 20 μL of methoxyamine hydrochloride in pyridine (40 mg mL^{-1}) was added to the dried sample and incubated for 90 min at 30 °C. Then, 80 μL of *N*-Methyl-*N*-trimethylsilyl trifluoroacetamide + 1% trimethylchlorosilane was added and incubated for 30 min at 37 °C. Fum (m/z = 346), FBP (m/z = 453),

mevalonate (m/z = 591), and their mass isotopomers were measured by the same GC/MS system as described above. The conditions for GC/MS analysis have been described elsewhere (Okahashi et al., 2015).

2.7. ^{13}C-metabolic flux analysis

The central carbon metabolic pathway of *E. coli* including glycolysis, the TCA cycle, the pentose phosphate pathway, the Entner-Doudoroff pathway, and anaplerotic reactions were considered for ^{13}C-MFA as described previously (Wada et al., 2017). Malate oxidoreductase was not considered for flux estimation because no enzyme activities of the crude cell extracts were observed under the all conditions (Table S2). Activities of NAD^+- and $NADP^+$-dependent malic oxidoreductase were measured as described previously (Wada et al., 2017). The list of reactions and its carbon atom transitions are shown in Table S3. The ^{13}C-enrichment of metabolites was calculated from a flux distribution using a model based on elementary metabolite units (Antoniewicz et al., 2007). Flux distribution was optimized to minimize the differences between measured and calculated ^{13}C-enrichments. Fitness was statistically evaluated by the χ^2 test with the standard deviation of ^{13}C-enrichment by GC/MS measurement at 0.02. The 95% confidence intervals of flux were estimated using the grid search method (Antoniewicz et al., 2006). All calculations were performed with OpenMebius (Kajihata et al., 2014) in MATLAB 2011b (Mathworks, Natick, MA, USA).

3. Results and discussion

3.1. Effect of nutrient starvation on mevalonate production

Mevalonate production was evaluated using an engineered *E. coli* possessing heterologous mevalonate synthetic pathway enzymes under nutrient starvation conditions. After growth on a normal synthetic medium, the obtained cells were inoculated into a fresh synthetic medium without nitrogen, sulfur, or magnesium, and aerobically cultured. The time courses of OD_{600} and concentrations of glucose, mevalonate, and acetate are shown in Fig. 1. The specific rates and carbon yields are summarized in Table 1. No decreases in OD_{600} and glucose consumption rates were observed until glucose depletion under all conditions. The results suggest that the cellular activities did not decrease and the steady-state conditions were maintained despite essential nutrient starvation. These specific glucose uptake rates under the stationary phases were lower than that under the growth phase. Glucose uptake rate was highest under the magnesium starvation, followed by sulfur starvation and the nitrogen starvation. This order was consistent with a previous study of a wild-type *E. coli* under various starvation conditions (Chubukov and Sauer, 2014).

As expected, mevalonate yield was greatly improved under any nutrient starvations compared to during the growth phase. This indicates that the carbon used for biomass synthesis during the growth phase was used for mevalonate synthesis in the stationary phase. Sulfur starvation resulted in the highest mevalonate yield (0.61 C-mol C-mol^{-1}) and specific production rate (2.17 mmol gDCW^{-1} h^{-1}). The yield reached 90% of its theoretical maximum value (0.67 C-mol C-mol^{-1}). This is also consistent with a previous report that mevalonate yield was highest under sulfur starvation conditions (Li et al., 2016). Furthermore, acetate production was observed under magnesium starvation. Because acetate is also synthesized from acetyl-CoA, byproduct formation must lead to reduced mevalonate yield. A yield of 0.60 C-mol C-mol^{-1} has been reported as the highest mevalonate yield by metabolic modification such as disrupting competing pathways and enhancing glucose uptake (Wang et al., 2016). Sulfur starvation showed similar performance for mevalonate production without additional genetic modifications.

Mevalonate yield differed depending on the type of restricted nutrients. To evaluate the causes of the different mevalonate yields under various starvation conditions, the enzyme amounts for catalyzing the mevalonate synthesis pathway, intracellular cofactor levels, and metabolic flux distribution were investigated.

3.2. Enzyme amounts for catalyzing the mevalonate synthesis pathway

Mevalonate synthesis is catalyzed by the heterologous enzymes, acetyl-CoA acetyltransferase/HMG-CoA reductase (MvaE) and HMG-CoA synthase (MvaS). Because the protein degradation must occur under the stationary phase with nutrient starvation, catalyst protein levels were evaluated by SDS-PAGE. Whole cell extract samples containing the same protein amounts were analyzed. Table 2 shows the relative abundance of mevalonate synthetic pathway enzymes obtained by image analysis of the band

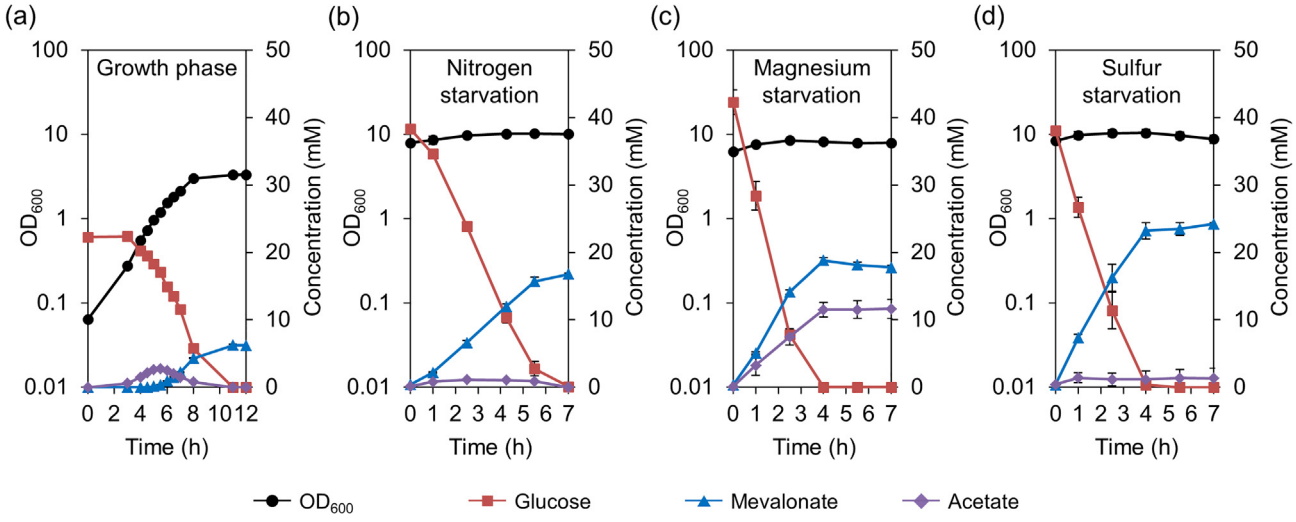

Fig. 1. Culture profiles of mevalonate-producing *E. coli* under growth phase (a), nitrogen starvation (b), magnesium starvation (c), or sulfur starvation (d). The circles, squares, triangles, and diamonds represent OD_{600}, glucose concentration, mevalonate concentration, and acetate concentration, respectively. Error bars are standard deviations of triplicate cultures. Note that, the data of growth phase (a) was modified as in previous report (Wada et al., 2017).

Table 1
Specific rates and carbon yields at growth phase and stationary phase.

	Growth phase	Stationary phase		
	Wada et al. (2017)	Nitrogen starvation	Magnesium starvation	Sulfur starvation
Glucose consumption (mmol $gDCW^{-1}$ h^{-1})	8.21 ± 0.22	2.43 ± 0.04	3.83 ± 0.30	3.64 ± 0.53
Growth rate (h^{-1})	0.48 ± 0.01	0.04 ± 0.03	0.03 ± 0.01	0.08 ± 0.02
Mevalonate production (mmol $gDCW^{-1}$ h^{-1})	1.84 ± 0.07	1.02 ± 0.03	1.86 ± 0.04	2.17 ± 0.34
Acetate production (mmol $gDCW^{-1}$ h^{-1})	0.00 ± 0.00	0.00 ± 0.00	1.12 ± 0.07	0.09 ± 0.13
Biomass yield (C-mol C-mol^{-1})	0.62 ± 0.00	0.12 ± 0.01	0.10 ± 0.01	0.11 ± 0.06
Mevalonate yield (C-mol C-mol^{-1})	0.22 ± 0.00	0.44 ± 0.00	0.45 ± 0.03	0.61 ± 0.02
Acetate yield (C-mol C-mol^{-1})	0.00 ± 0.00	0.00 ± 0.00	0.09 ± 0.01	0.01 ± 0.01

Table 2
Relative abundance of the mevalonate synthetic pathway enzymes.

Enzyme	Nitrogen starvation		Magnesium starvation		Sulfur starvation	
	1 h	3 h	1 h	3 h	1 h	3 h
MvaE	0.68	0.58	0.66	0.71	1.06	0.92
MvaS	0.99	0.91	0.98	1.45	1.36	1.54

density to the total protein (Schneider et al., 2012). The SDS-PAGE image is shown in Fig. S1. Although no decrease in MvaS level was observed under all conditions, MvaE level decreased under nitrogen or magnesium starvations. Particularly, the abundance of MvaE under nitrogen starvation decreased to 58% of that of the growth phase. In contrast, no decrease in MvaE abundance was observed under sulfur starvation.

Nitrogen is an essential component of all proteins and accounts for approximately 15% of the elemental composition of proteins. It has been reported that many amino acids show decreased levels during nitrogen starvation and are deaminated to generate usable nitrogen (Brauer et al., 2006). Because the mevalonate-producing strain overexpresses heterologous enzymes, these abundant proteins must be easily decomposed under nitrogen starvation condition.

3.3. Effect of nutrient starvation on intracellular NADPH/$NADP^+$ ratio

Because the mevalonate synthesis pathway requires NADPH as the reductive power, the NADPH/$NADP^+$ ratio may affect mevalonate production as the driving force. Intracellular cofactors concentrations were measured by enzymatic assay (Table 3). As particularly large ratio of NADPH/$NADP^+$ was observed under nitrogen starvation. Furthermore, there was no considerable difference in NADPH concentration under any of the conditions. Because mevalonate production under sulfur starvation was the highest, these results suggest that excess NADPH does not promote mevalonate synthesis.

Table 3
Concentration of cofactors under the nutrient starvation conditions.

	Nitrogen starvation	Magnesium starvation	Sulfur starvation
NADPH (μmol $gDCW^{-1}$)	1.04 ± 0.06	1.06 ± 0.13	0.96 ± 0.07
$NADP^+$ (μmol $gDCW^{-1}$)	0.63 ± 0.01	1.14 ± 0.06	0.98 ± 0.02
NADH (μmol $gDCW^{-1}$)	2.14 ± 0.56	1.10 ± 0.71	1.65 ± 0.02
NAD^+ (μmol $gDCW^{-1}$)	5.04 ± 0.18	5.93 ± 0.15	5.29 ± 0.19
NADPH/$NADP^+$	1.66 ± 0.07	0.93 ± 0.16	0.98 ± 0.09
NADH/NAD^+	0.42 ± 0.11	0.19 ± 0.12	0.31 ± 0.01

NADH/NAD^+ was particularly low under magnesium starvation, and the largest under nitrogen starvation. It has been reported that low NADH/NAD^+ increases glycolytic flux in *E. coli* (Zhu et al., 2008). The result supports that the specific glucose uptake rate was high under magnesium starvation and low under nitrogen starvation (Table 1).

3.4. Flux distributions under nutrient starvation conditions

One molecule of mevalonate is synthesized from 3 molecules of acetyl-CoA using 2 molecules of NADPH. The supplies of acetyl-CoA and NADPH are expected to affect mevalonate yield. Because NADPH is produced in some reactions such as glucose-6-phosphate dehydrogenase (G6PDH), 6-phosphogluconate dehydrogenase (6PGDH), isocitrate dehydrogenase (ICDH), malate oxidoreductase (ME), and transhydrogenase (TDH) in the central carbon metabolism, these fluxes were determined by ^{13}C-MFA. Flux distribution was estimated based on ^{13}C-enrichment of intermediates of the cells cultured using [1-^{13}C] glucose. Because no specific activities of malate oxidoreductase for both types were confirmed by *in vitro* enzymatic assays (Table S2), the reaction was not considered for flux estimation.

^{13}C-enrichments of FBP, 3PG, PEP, Cit, Fum, and mevalonate at 2.5 and 3.5 h during the stationary phase were measured by GC/MS, and the isotopic steady state was confirmed. Because the degree of freedom of the model for ^{13}C-MFA was 18 and the number of fragments used for optimization was 37, the threshold for the χ^2 test was 30.14. Fitness of ^{13}C-enrichments of metabolites at the estimated flux distribution under nitrogen, magnesium, and sulfur starvation conditions were 13.00, 6.65, and 10.70, respectively, and passed the χ^2 test. The flux distributions and ^{13}C-enrichments of metabolites under nutrient starvation conditions are shown in Fig. 2 and Table S4.

Under nitrogen starvation, 45% of the uptake glucose was metabolized via glycolysis and the remaining 55% was used in the pentose phosphate pathway. The proportion via the pentose

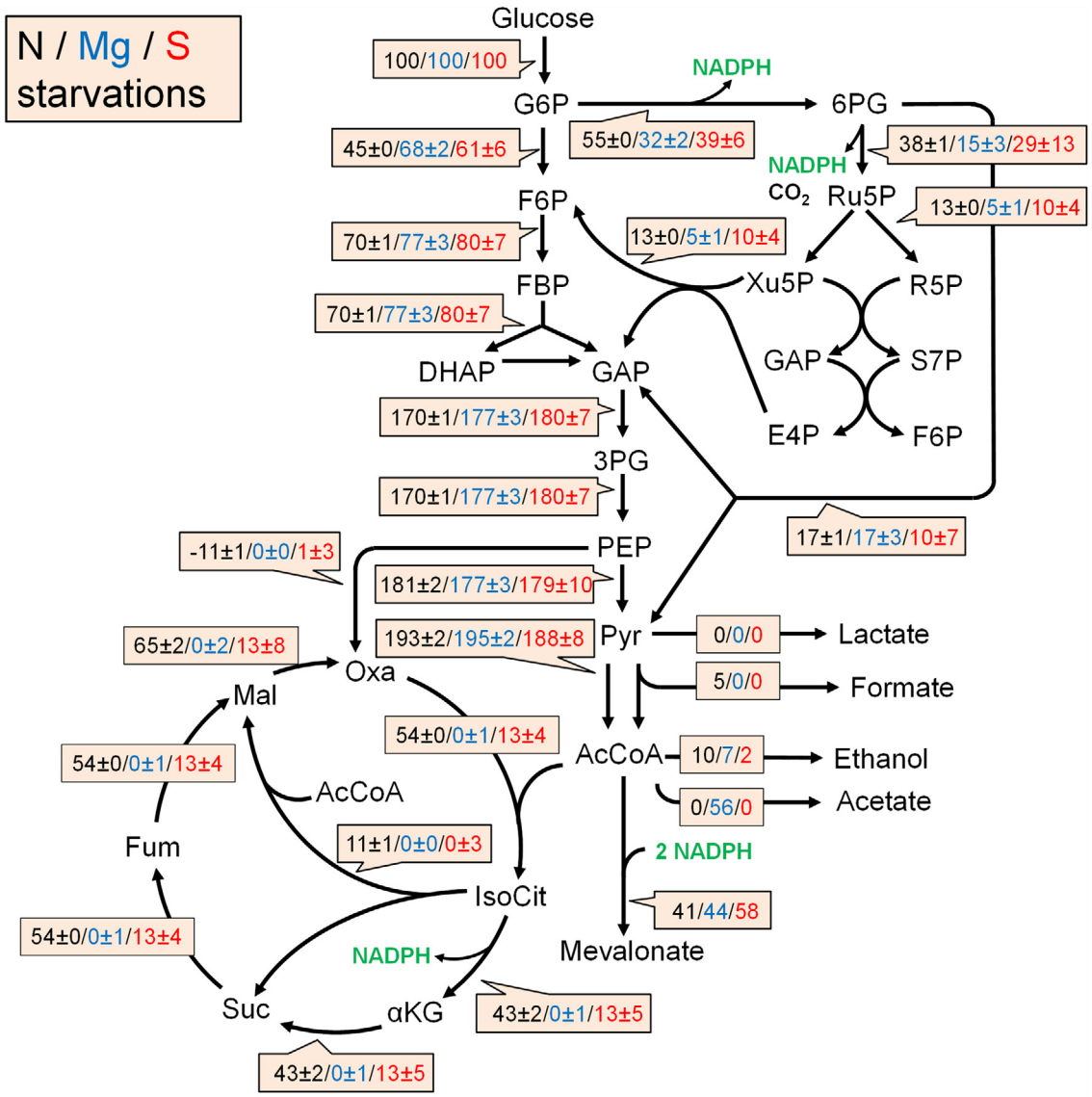

Fig. 2. Flux distributions of mevalonate producing *E. coli* under nutrient starvation. Estimated flux and its standard deviation were normalized to a glucose uptake rate of 100. The standard deviation was calculated with the 95% confidence interval of the corresponding flux.

phosphate pathway was 32% under magnesium starvation, indicating lower NADPH production. The precursor of mevalonate, acetyl-CoA, is synthesized by pyruvate dehydrogenase and pyruvate formate lyase in *E. coli*. Total acetyl-CoA production flux under nitrogen, magnesium, and sulfur starvation were 198 ± 2%, 195 ± 2%, and 188 ± 8%, respectively. There was no notable difference in flux of acetyl-CoA synthesis. Flux of the TCA cycle was the highest under nitrogen starvation, and was lower under magnesium and sulfur starvation. Because the TCA cycle flux is accompanied by CO_2 emission, low mevalonate yield was achieved under nitrogen starvation. Under nitrogen starvation, a decrease in the enzyme amount of overexpressed MvaE was observed (Table 2). The decrease in the mevalonate synthesis pathway enzymes would have promoted increased carbon flow to competitive pathways. In contrast, the TCA cycle flux was suppressed under sulfur or magnesium starvation. It has been reported that several enzymes of the TCA cycle such as aconitase, fumarase and succinate dehydrogenase require Fe-S clusters for their activity (Johnson et al., 2005). Because sulfur starvation affects synthesis of the Fe-S cluster, the TCA cycle flux would be restricted. Magnesium is known as a cofactor of isocitrate dehydrogenase and succinyl-CoA synthase in the TCA cycle (Fraser et al., 1999; Oudot et al., 2001). Reductions of these enzyme activities would decrease TCA cycle flux.

3.5. NADPH production/consumption balances

Based on the estimated flux distributions, the flux of NADPH production/consumption via the central carbon metabolism was calculated (Fig. 3). Considering the mass balance of NADPH under the steady state, the gap between production and consumption was regarded as the contribution of transhydrogenase (TDH). Total NADPH production was the highest under nitrogen starvation and the lowest under magnesium starvation. Because total NADPH production was higher than NADPH consumption for mevalonate synthesis under nitrogen starvation, TDH functioned in NADPH oxidation. In contrast, because the NADPH consumption for mevalonate synthesis was larger than NADP production in the central carbon metabolism under magnesium starvation and sulfur starvation, TDH functioned in the direction of NADPH formation. These results are consistent with the fact that the NADPH/$NADP^+$ ratio was the highest under nitrogen starvation (Table 3).

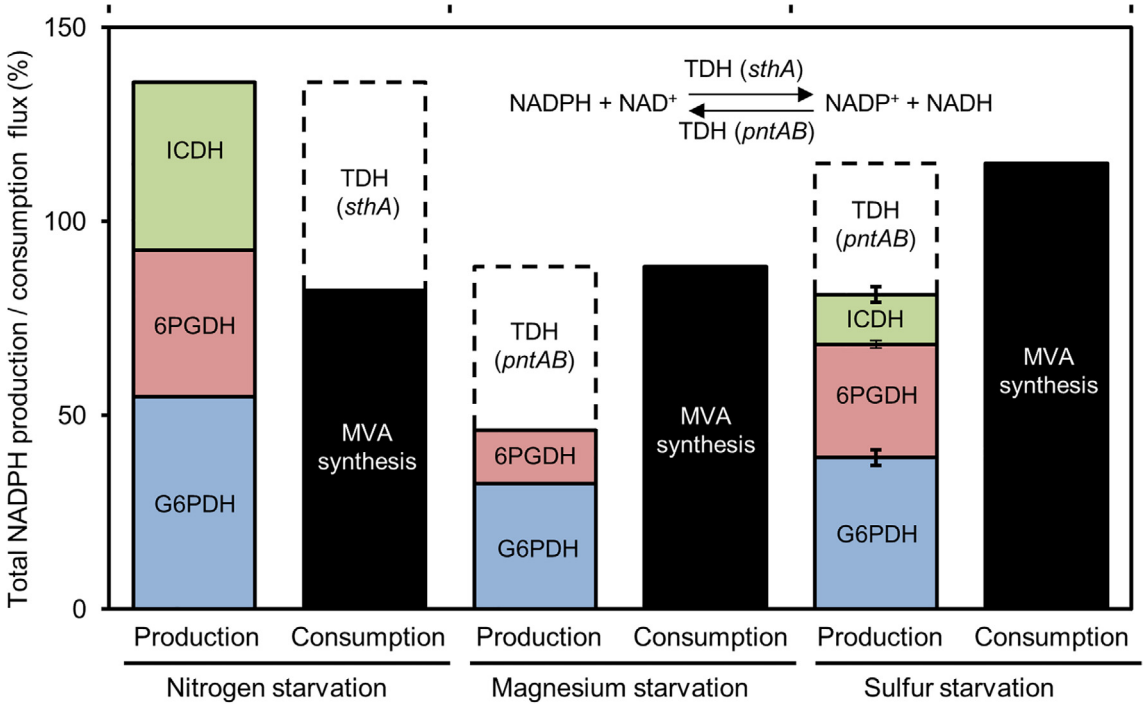

Fig. 3. Balance of NADPH production/consumption flux. Each flux value was normalized to a glucose uptake rate of 100. Error bars are the 95% confidence interval of the corresponding flux.

Under magnesium starvation, mevalonate yield decreased because of the production of acetate which is synthesized from the same precursor, acetyl-CoA (Table 1). NADPH is a required cofactor for mevalonate synthesis, whereas it is not necessary for acetate synthesis. ^{13}C-MFA revealed that the total flux of NADPH production from the central carbon metabolism was the lowest under magnesium starvation conditions. Therefore, sufficient amounts of acetyl-CoA could not be drawn into the mevalonate synthesis pathway sufficiently because of the shortage of NADPH supply. Furthermore, because the enzyme activities of the TCA cycle were suppressed, acetyl-CoA overflowed into the acetate synthesis pathway. The low NADPH production under magnesium starvation was due to the low flux of the oxidative pentose phosphate pathway (Fig. 4). It has been reported that magnesium acts as a cofactor in many phosphorylation and dephosphorylation reactions (Fox et al., 2001). Magnesium starvation also affected enzyme activity in the oxidative pentose phosphate pathway.

Under sulfur starvation, no decomposition of overexpressed enzymes was observed. Additionally, ^{13}C-MFA revealed that the TCA cycle flux was suppressed and the total NADPH production flux was 1.8-fold higher than that under magnesium starvation. Such high mevalonate yield occurred because there was no negative factor in mevalonate production in terms of the supplies of acetyl-CoA and NADPH and maintenance of enzyme amount for mevalonate synthesis under sulfur starvation.

3.6. Deletion of NADPH producing reactions under sulfur starvation

The ^{13}C-MFA suggested that the contributions of the pentose phosphate pathway and TDH were large in the production of

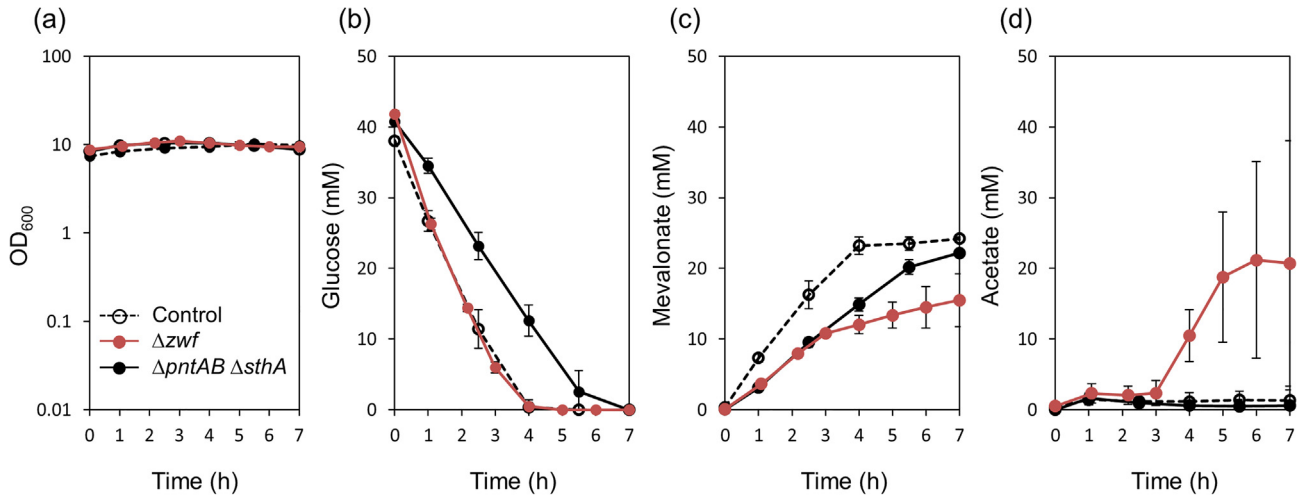

Fig. 4. Effect of G6PDH and TDH deletions under sulfur starvation. (a) OD_{600}, (b) glucose concentration, (c) mevalonate concentration, and (d) acetate concentration. Open circle, closed circle, and red-filled circle represent the mevalonate producing strain, its G6PDH (encoded by *zwf*), and TDH (encoded by *pntAB* and *sthA*) deletion mutants, respectively. Error bars are standard deviations of triplicate cultures. (For interpretation of the references to colour in this figure legend, the reader is referred to the web version of this article.)

NADPH under sulfur starvation (Fig. 3). To confirm this result, metabolic changes following the deletion of enzymes that catalyze these reactions were investigated. The culture profiles of a mevalonate-producing strain and its Δ*zwf* mutant and Δ*pntAB* Δ*sthA* mutant are shown in Fig. 4.

Deletion of *zwf*, which encodes G6PDH, caused a decrease in mevalonate yield and increase in acetate yield. Deletion of *pntAB* and *sthA*, encoding TDH, decreased the glucose uptake rate. Although the mevalonate production rate also decreased, the yield did not change. Furthermore, no acetate production was observed in the Δ*pntAB* Δ*sthA* mutant. These results suggest that the pentose phosphate pathway is the primary reaction involved in NADPH production in *E. coli* under sulfur starvation. Inactivation of the pentose phosphate pathway must cause a shortage of NADPH for mevalonate production. Therefore, the *zwf* deletion mutant showed an overflow in acetate for the same reason as during magnesium starvation. Thus, the parent strain could produce sufficient NADPH for mevalonate synthesis.

It is important to maintain a low NADH/NAD^+ ratio to achieve high glycolysis flux (Zhu et al., 2008). The mevalonate-producing strain can control the NADH/NAD^+ ratio by converting excess NADH produced in glycolysis to NADPH by TDH under sulfur starvation. Because excess NADH could not be converted to NADPH in the TDH deletion mutant, the glucose uptake rate decreased. Low glycolysis flux would alleviate the NADPH shortage and prevent the decrease in mevalonate yield.

3.7. Toward production of other targets under nutrient starvations

In the present study, the metabolic impacts of nutrient starvation were investigated by ^{13}C-MFA. These findings suggest that sulfur starvation is suitable for producing compounds, such as 3-hydroxypropionate, fatty acids, and isopropanol, which are synthesized from acetyl-CoA using NADPH as a cofactor (Hanai et al., 2007; Liu et al., 2010; Rathnasingh et al., 2012). However, sulfur starvation is not suitable for producing targets synthesized from intermediates of the TCA cycle. These compounds can be produced under nitrogen starvation with controlling the degradation of overexpressed enzymes. Although magnesium starvation is not suitable for producing mevalonate because of the NADPH supply shortage, the large glycolysis flux is attractive. Magnesium starvation is an effective approach for producing targets that are synthesized from glycolytic intermediates without NADPH.

4. Conclusions

In the present study, mevalonate yield in an engineered *E. coli* strain was enhanced by growth inhibition under essential nutrient starvation conditions. Sulfur starvation resulted in the highest mevalonate yield of 0.61 C-mol C-mol-1 (90% of theoretical maximum value). The reasons for the suitability of sulfur starvation for mevalonate production were clarified by determining metabolic flux distribution. Suppression of the TCA cycle flux and sufficient NADPH production for mevalonate synthesis was the reason to achieve such the high mevalonate yield under sulfur starvation.

Acknowledgements

We thank Prof. Fumio Matsuda for (Osaka University, Japan) for their helpful comments. This work was supported by Grant-in-Aid for Scientific Research (B) No. 16H04576. It was also supported by Grant-in-Aid for Young Scientists (B) No. 16K18298.

Appendix A. Supplementary data

Supplementary data associated with this article can be found, in the online version, at http://dx.doi.org/10.1016/j.biortech.2017.04.110.

References

Antoniewicz, M.R., Kelleher, J.K., Stephanopoulos, G., 2006. Determination of confidence intervals of metabolic fluxes estimated from stable isotope measurements. Metab. Eng. 8, 324–337.
Antoniewicz, M.R., Kelleher, J.K., Stephanopoulos, G., 2007. Elementary metabolite units (EMU): a novel framework for modeling isotopic distributions. Metab. Eng. 9, 68–86.
Brauer, M.J., Yuan, J., Bennett, B.D., Lu, W., Kimball, E., Botstein, D., Rabinowitz, J.D., 2006. Conservation of the metabolomic response to starvation across two divergent microbes. Proc. Natl. Acad. Sci. U.S.A. 103, 19302–19307.
Chubukov, V., Sauer, U., 2014. Environmental dependence of stationary-phase metabolism in *Bacillus subtilis* and *Escherichia coli*. Appl. Environ. Microbiol. 80, 2901–2909.
Datsenko, K.A., Wanner, B.L., 2000. One-step inactivation of chromosomal genes in *Escherichia coli* K-12 using PCR products. Proc. Natl. Acad. Sci. U.S.A. 97, 6640–6645.
Doucette, C.D., Schwab, D.J., Wingreen, N.S., Rabinowitz, J.D., 2011. α-Ketoglutarate coordinates carbon and nitrogen utilization via enzyme I inhibition. Nat. Chem. Biol. 7, 894–901.
Fox, C., Ramsoomair, D., Carter, C., 2001. Magnesium: its proven and potential clinical significance. South. Med. J. 94, 1195–1201.
Fraser, M.E., James, M.N., Bridger, W.A., Wolodko, W.T., 1999. A detailed structural description of *Escherichia coli* succinyl-CoA synthetase. J. Mol. Biol. 285, 1633–1653.
Hanai, T., Atsumi, S., Liao, J.C., 2007. Engineered synthetic pathway for isopropanol production in *Escherichia coli*. Appl. Environ. Microbiol. 73, 7814–7818.
Johnson, D.C., Dean, D.R., Smith, A.D., Johnson, M.K., 2005. Structure, function, and formation of biological iron-sulfur clusters. Annu. Rev. Biochem. 74, 247–281.
Kajihata, S., Furusawa, C., Matsuda, F., Shimizu, H., 2014. OpenMebius: an open source software for isotopically nonstationary ^{13}C-based metabolic flux analysis. Biomed. Res. Int. 2014, 627014.
Kuzuyama, T., Dairi, T., Yamashita, H., Shoji, Y., Seto, H., 2004. Heterologous mevalonate production in *Streptomyces lividans* TK23. Biosci. Biotechnol. Biochem. 68, 931–934.
Kuzuyama, T., Hemmi, H., Takahashi, S., 2010. Mevalonate pathway in bacteria and archaea. In: Mander, L., Liu, H.W. (Eds.), Comprehensive Natural Products II, vol. 1. Elsevier, Oxford, pp. 493–516.
Li, S., Jendresen, C.B., Nielsen, A.T., 2016. Increasing production yield of tyrosine and mevalonate through inhibition of biomass formation. Proc. Biochem. 51, 1992–2000.
Liu, T., Vora, H., Khosla, C., 2010. Quantitative analysis and engineering of fatty acid biosynthesis in *E. coli*. Metab. Eng. 12, 378–386.
Okahashi, N., Kohno, S., Kitajima, S., Matsuda, F., Takahashi, C., Shimizu, H., 2015. Metabolic characterization of cultured mammalian cells by mass balance analysis, tracer labeling experiments and computer-aided simulations. J. Biosci. Bioeng. 120, 725–731.
Oudot, C., Cortay, J.C., Blanchet, C., Laporte, D.C., Di Pietro, A., Cozzone, A.J., Jault, J. M., 2001. The "catalytic" triad of isocitrate dehydrogenase kinase/phosphatase from *E. coli* and its relationship with that found in eukaryotic protein kinases. Biochemistry 2001 (40), 3047–3055.
Rathnasingh, C., Raj, S.M., Lee, Y., Catherine, C., Ashok, S., Park, S., 2012. Production of 3-hydroxypropionic acid via malonyl-CoA pathway using recombinant *Escherichia coli* strains. J. Biotechnol. 157, 633–640.
Schneider, C.A., Rasband, W.S., Eliceiri, K.W., 2012. NIH Image to ImageJ: 25 years of image analysis. Nat. Methods 9, 671–675.
Shimizu, K., 2013. Regulation Systems of Bacteria such as *Escherichia coli* in Response to Nutrient Limitation and Environmental Stresses. Metabolites 4, 1–35.
Tabata, K., Hashimoto, S., 2004. Production of mevalonate by a metabolically-engineered *Escherichia coli*. Biotechnol. Lett. 26, 1487–1491.
Tamura, G., Ando, K., Kodama, K., Arima, K., 1968. Production of mevalonic acid by fermentation. Appl. Microbiol. 16, 965–972.
Wada, K., Toya, Y., Banno, S., Yoshikawa, K., Matsuda, F., Shimizu, H., 2017. ^{13}C-metabolic flux analysis for mevalonate-producing strain of *Escherichia coli*. J. Biosci. Bioeng. 123, 177–182.
Wang, J., Niyompanich, S., Tai, Y.S., Wang, J., Bai, W., Mahida, P., Gao, T., Zhang, K., 2016. Engineering of a highly efficient *Escherichia coli* strain for mevalonate fermentation through chromosomal integration. Appl. Environ. Microbiol. 82, 7176–7184.
Xiong, M., Schneiderman, D.K., Bates, F.S., Hillmyer, M.A., Zhang, K., 2014. Scalable production of mechanically tunable block polymers from sugar. Proc. Natl. Acad. Sci. U.S.A. 111, 8357–8362.
Zhu, Y., Eiteman, M.A., Altman, R., Altman, E., 2008. High glycolytic flux improves pyruvate production by a metabolically engineered *Escherichia coli* strain. Appl. Environ. Microbiol. 74, 6649–6655.